Applied Surface Science Advances 29 (2025) 100842

Contents lists available at ScienceDirect

Applied Surface Science Advances

journal homepage: www.sciencedirect.com/journal/applied-surface-science-advances

Full Length Article

Rational material design of chemically inert oxide anode coating layers for lithium metal and all-solid-state batteries

Dong Won Jeon [a,b], Wootaek Choi [d], Jun Hyuk Kang [a,b], Hyeon Woo Kim [b,c], Min Sung Kang [a,b], Woongchan Kim [a,b], Han Uk Lee [a,b], Hyunseok Ko [f], Patrick Joohyun Kim [d,e,*], Sung Beom Cho [a,b,c,*]

[a] Department of Energy Systems Research, Ajou University, Suwon 16499, Republic of Korea
[b] Department of Materials Science and Engineering, Ajou University, Suwon 16499, Republic of Korea
[c] Ajou Energy Science Research Center, Ajou University, Suwon 16499, Republic of Korea
[d] School of Semiconductor Convergence Engineering, Kyungpook National University, Daegu 41566, Republic of Korea
[e] School of Chemical Engineering and Applied Chemistry, Kyungpook National University, Daegu 41566, Republic of Korea
[f] Division of Carbon Neutrality & Digitalization, Korea Institute of Ceramic Engineering and Technology (KICET), Jinju 52851, Republic of Korea

ARTICLE INFO

Keywords:
All-Solid-State battery
Anode coatings
High-throughput screening
DFT calculations
FEM simulations
Machine-learning tools

ABSTRACT

While many coating materials have been explored to address the compatibility issues between Li anodes and solid-state electrolytes, a fully tailored material has yet to be suggested. Herein, we systematically evaluated potential coating candidate material properties to establish effective guidelines for functional battery material discovery. By performing high-throughput screening with various methodologies, we identified promising coating candidates such as $LiTbO_2$, and $LiDyO_2$, which exhibit inhibition of Li dendrite growth, non-reactivity, lithiophilicity, and sufficient ionic conductivity. Additionally, instead of directly synthesizing the coating layer from commercialized binary precursors, we experimentally induced the coating layers $LiTbO_2$ and $LiDyO_2$ from the binaries within the cell and validated their potential as coatings. Our findings provide a systematic framework for discovering and developing new materials to enhance the performance, safety, and commercial viability of all solid-state batteries.

1. Introduction

All solid-state batteries (ASSBs) are emerging as a promising alternative to conventional liquid electrolyte batteries, as they address safety concerns associated with flammable organic compounds and potential energy density issues by utilizing lithium metal [1]. In recent years, significant advancements in synthesis and computational science technologies have led to the development of a large number of solid-state electrolytes (SEs) with these advantages. Among them, sulfide-SEs such as $Li_{10}GeP_2S_{12}$ [2] and $Li_{9.54}Si_{1.74}P_{1.44}S_{11.7}Cl_{0.3}$ [3] are gaining attention as promising next-generation battery materials due to their high ionic conductivity comparable to conventional liquid electrolytes [2,4]. Other examples, such as garnet-type electrolytes like $Li_7La_3Zr_2O_{12}$, show high chemical stability and a wide electrochemical window [5]. However, despite these advantages, most SEs have limited compatibility with lithium metal, leading to overall battery performance degradation due to issues such as contact problems, unintended side reactions, and Li dendrite growth [6–9]. This limited compatibility stems from the tendency of various SEs to exhibit poor wettability and high reactivity with lithium metal, influenced by complex interface physics and chemistry simultaneously [10–12]. Therefore, overcoming these incompatibility issues between SEs and lithium metal is a crucial challenge for the commercialization of ASSBs, and one effective solution is the introduction of an anode coating layer [13,14].

By introducing a coating layer, numerous attempts have been made to suppress Li dendrite formation and prevent SE decomposition, which are the most serious problems in the ASSB system. A significant factor in Li dendrite formation stems from interface issues between Li and SEs. Inadequate interface contact can lead to irregular lithium stripping and deposition during battery cycling, resulting in localized current density variations [10]. This condition exacerbates Li dendrite formation and hastens interface failure. To solve this issue, introducing a lithiophilic coating material is considered a promising solution because it can alleviate the interface contact problem and suppress Li dendrite growth

* Corresponding authors.
E-mail addresses: pjkim@knu.ac.kr (P.J. Kim), csb@ajou.ac.kr (S.B. Cho).

https://doi.org/10.1016/j.apsadv.2025.100842
Received 23 May 2025; Received in revised form 21 August 2025; Accepted 31 August 2025
Available online 9 September 2025

to some extent. For instance, materials like Al_2O_3, ZnO, and Au offer excellent wettability with lithium metal, ensuring good interface contact [15–18]. However, the major drawback is their potential reactivity with lithium metal, which may lead to the formation of undesired secondary phases [19]. These interphases can increase interface impedance or promote SE decomposition, depending on the type of secondary phase formed. The decomposition of electrolytes is usually caused by high reactivity with lithium. To prevent SE decomposition, a thermodynamically stable buffer layer can be introduced at the Li and SE interface. Li binary compounds such as LiX (X = F, Cl, Br), Li_2O, LiH, and Li_3N are thermodynamically stable with lithium metal. Since they do not react with lithium metal, they can act as a buffer layer to isolate SEs from the Li anode [12]. However, the ionic conductivity of Li binary compounds is unacceptably low, so they can only serve as very thin protective layers for lithium metal, potentially hindering overall cell performance [12]. Finding good coating materials also requires other criteria such as mechanical properties, electrochemical stability, lithiophilicity with lithium metal, interfacial stability, and ease of Li^+ transport. Various materials have been proposed as coatings to address the major issues in ASSBs, but a tailored material that meets all the requirements has yet to be identified. Therefore, a thorough investigation is necessary to find materials that can meet the diverse requirements across various fields.

In this study, we conducted high-throughput screening to establish efficient guidelines for investigating new materials and discovering promising candidates for anode coating. To begin with, we delved into the Materials Project (MP) database [20], specifically targeting chemical systems of Li-containing ternary oxides that could potentially leverage transport channels constructed by the Li sublattice. Subsequently, we employed multiple techniques, such as Density Functional Theory (DFT), machine learning model, and Finite Element Method (FEM), to analyze various material properties. We systematically evaluated the coating candidates using various calculation methods to assess phase stability, mechanical properties, electrochemical stability, lithiophilicity, interface stability, and ion migration energy. Through this workflow, we identified several promising anode coating materials, including $LiTbO_2$, and $LiDyO_2$, which met all the above criteria simultaneously. Furthermore, by fabricating half-cells and evaluating their cycling performance and chemical inertness, we confirmed their promising potential as coating layers. Our study may inspire the development of ASSBs by highlighting new functional materials that have been previously overlooked for battery applications.

2. Results

2.1. Database screening

Material screening was conducted through several steps, as shown in Figure 1. The screening criteria include commercial availability, mechanical properties, electrochemical stability, interface-related properties such as lithiophilicity and interphase evolution, and Li-ion migration energy. As a first step, Li-M-O ternary oxide systems were chosen as candidates for anode coating due to their abundance in the MP database, surpassing chlorides and fluorides. We initiated database screening by excluding components containing toxic, radioactive, and precious elements, considering commercial utilization. Additionally, during battery cycling, electron inflow into the cell must be blocked to prevent Li dendrite growth or decomposition of SEs. To screen out electronically conductive materials, we utilized Kohn-Sham (K-S) band gap data derived from DFT calculations, which is underestimated compared to experimental values, as a primary criterion. Using band gap data from the MP, we deprecated potentially electronically conductive materials with a bandgap below 0.5 eV [21]. Furthermore, the anode coating materials must maintain their structural stability, which can be assessed by their phase stability [22]. In this step, candidates were deemed thermodynamically stable if $E_{hull} \leq 0.005$ eV/atom, potentially stabilized by entropic effects at room temperature [23]. Among the 2, 192 unfiltered Li-M-O ternary systems, these initial screening criteria yielded only 147 compounds with unique composition for further consideration of mechanical properties.

2.2. Mechanical properties

The growth of Li dendrites presents a significant challenge in battery systems due to their potential to cause short-circuiting by extending into the cathode [24,25]. This process involves a complex interplay of electrochemical, chemical, and mechanical factors, making it one of the most intricate phenomena in battery systems [26]. While the exact

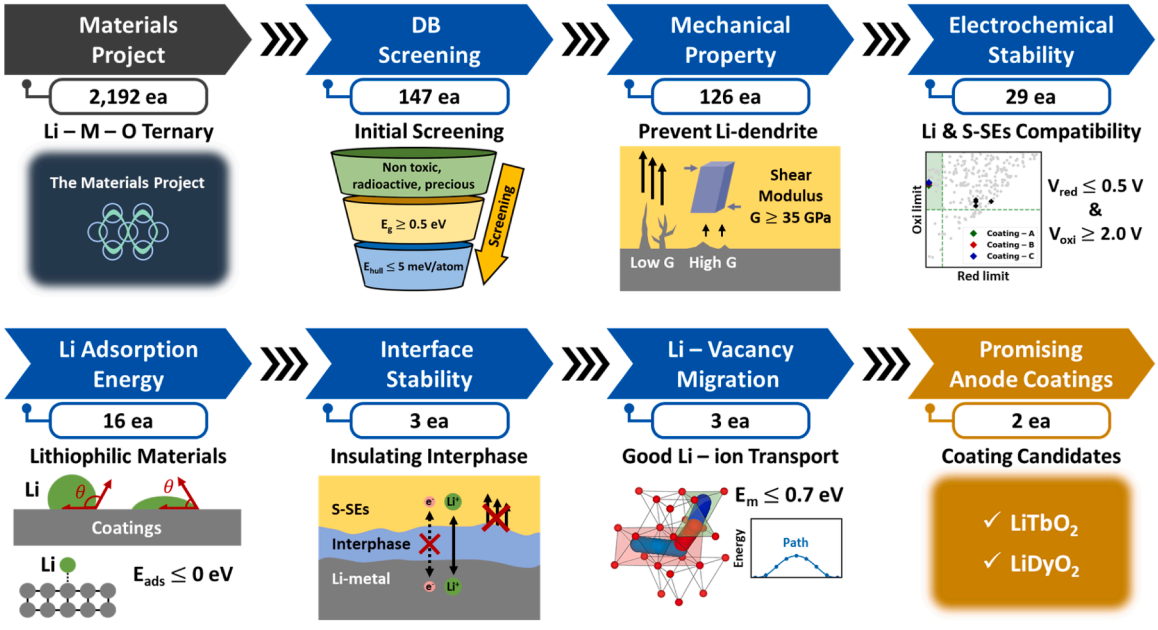

Fig. 1. Computational screening workflow for lithium and SEs compatible coating layer. The number of candidates that passed the screening criteria is displayed at the top center of each step.

mechanism of dendrite formation and growth is not fully understood, prior research has highlighted the importance of both electronic conductivity and mechanical properties [12]. Monroe and Newman suggested that the shear modulus is one of the key factors in effectively suppressing Li dendrite growth [27]. LiPON thin-film coatings, characterized by a shear modulus of 31 GPa — nearly nine times that of lithium metal (≈ 3.4 GPa) — exhibited no observable Li dendrite formation during cycling in the SEs, supporting the significant influence of the coating layer's shear modulus on dendrite growth inhibition [28]. In comparison, sulfide-based electrolytes such as LGPS and LPSCl have much lower shear modulus values of 7.9 [29] and 8.1 [29] GPa, respectively, making them more susceptible to dendrite formation and growth. Conversely, oxide-based electrolytes like LLZO and LTPO, with shear modulus of 59.6 [30] and 55.6 [29] GPa, respectively, have shear modulus nearly twice that of LiPON, and are predicted to be more favorable for dendrite growth suppression.

Recently, the elastic behavior of inorganic SEs has been found to play a major role in the stability of electrodeposition at interfaces within solid electrolytes [31,32]. Thereby, the elastic tensor serves as an excellent screening criterion for battery material discovery or design, as it correlates with the dendrite issue [33]. However, despite the significance of elastic tensors, calculating them using ab-initio methods still requires substantial computational resources, with data available for only 6.6 % of the MP database [34,35]. To rapidly and accurately estimate the elastic tensor of candidate materials, we employed the equivariant graph neural network-based Materials Tensor model (MatTen) [35]. We used MatTen to obtain the full elastic tensor of the candidate materials, which was used to calculate the Voigt-Reuss-Hill (VRH) shear modulus for their evaluation. Screening criteria were set at 35 GPa, over ten times that of Li metal, and candidates that passed this threshold were expected to impede Li dendrite growth with similar performance to LiPON [28]. Using this criterion, we were able to narrow down 126 compounds that satisfied the shear modulus criterion from a total of 147 candidates.

To gain further insight into the impact of shear modulus on Li dendrite growth during battery cycling, Finite Element Method (FEM) simulations were conducted. Assuming identical triangular cap-shaped nuclei with a width of 10 nm as depicted in Fig. 2b-c, the evolution of these nuclei was simulated over 450 seconds to focus on the dendrite growth effect. The detailed equations and parameters used in the simulations are provided in the Methods section of supplementary materials and Table S1, respectively. Figure 2a illustrates the shear modulus distribution of candidates that passed the DB screening. The shear modulus value of the candidates approximately ranges from 0 GPa to 120 GPa and the median value is close to 60 GPa, well above the screening criteria and representing the most common candidates. We used this median value to FEM simulate the extent of dendrite growth to ensure the effectiveness of the criteria of shear modulus. Fig. 2b shows the simulation results for the situation without coating material, where the calculated shear modulus of LGPS (≈ 8 GPa) was applied. Conversely, Figure 2c shows simulation results when a coating material with a median shear modulus value was used. In the situation where no coating was applied (Fig. 2b), non-uniform Li deposition and dendrite shapes were observed on the Li interface. In contrast, a coating layer with a high shear modulus (Figure 2c) promotes a relatively smooth geometry through uniform Li deposition. Thus, a coating film with a higher shear modulus is advantageous in suppressing Li dendrite growth [36–38]. The simulation geometry and corresponding results for various shear modulus values are presented in Figure S1.

2.3. Electrochemical stability

The electrochemical stability window of a material denotes the voltage range (in comparison to Li metal) wherein the material remains resistant to decomposition [39,40]. Hence, an effective coating layer should have a sufficiently wide electrochemical stability window to prevent redox reactions at the interface. By calculating the reduction and oxidation limits of coating candidates, we can assess their suitability for anode coating. To estimate these limits, we constructed a grand potential phase diagram Φ of the compounds based on the chemical potential of Li [41,42].

Employing this approach, we illustrated the reduction and oxidation limits of all the candidates in Fig. 3a. The reduction limit criterion was set below 0.5 V and the oxidation limit criterion was set above 2.0 V to ensure minimum compatibility with the Li metal anode and SEs. These criteria allowed us to narrow down the candidates that met the electrochemical stability requirements to a total of 29. Among these candidates, several materials with a 0 V reduction limit that can maintain electrochemical stability with lithium metal are shown in Fig. 3b. For example, the reduction limit of $LiTbO_2$ and $LiDyO_2$ is 0 V, and simultaneously, E_{hull} is 0 eV/atom, indicating their inertness to lithium metal from both thermodynamic and electrochemical perspectives during battery cycling. As another example, Li_8HfO_6 is thermodynamically metastable (E_{hull} = 0.003 eV/atom), its reduction limit of 0 V suggests stability with Li metal concerning electrochemical stability. If Li_8HfO_6 can be synthesized and maintain a metastable phase during operation, it holds promise as an anode coating. The oxidation limits of these three materials are close to 3 V, higher than the oxidation limits of many well-known SEs, so they are expected to be compatible with most SEs.

2.4. Li adsorption energy and interface stability

A recent study has proposed strategies to suppress vertical lithium dendrite growth by inserting interlayers between solid electrolytes [43]. These interlayers redistribute the current density concentrated at the dendrite tip, thereby preventing further propagation. To ensure uniform current distribution at the interface between the Li anode and the

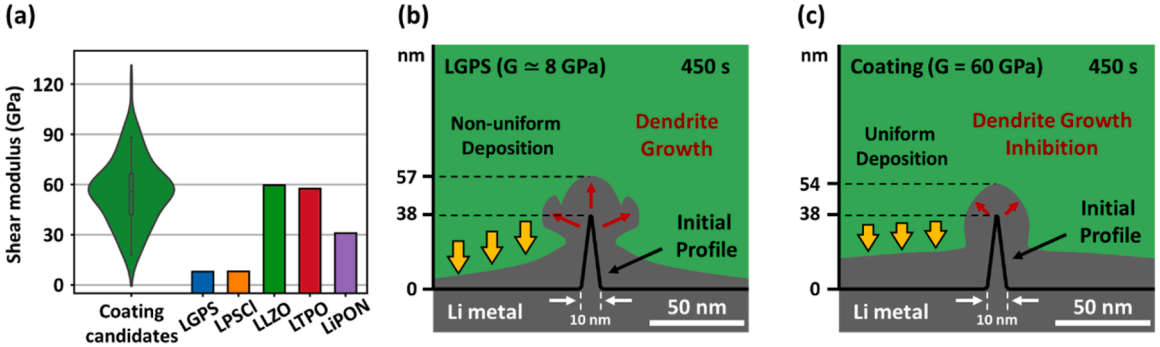

Fig. 2. (a) Distribution of shear modulus for 147 candidate coating materials (green violin plot) compared to representative solid electrolyte materials (colored bar graph). The violin plot illustrates the variability and median of shear modulus among coating candidates, while the bars represent typical values for well-known electrolytes. (b) Li dendrite growth simulation within LGPS bulk. (c) Li dendrite growth simulation within coating candidates.

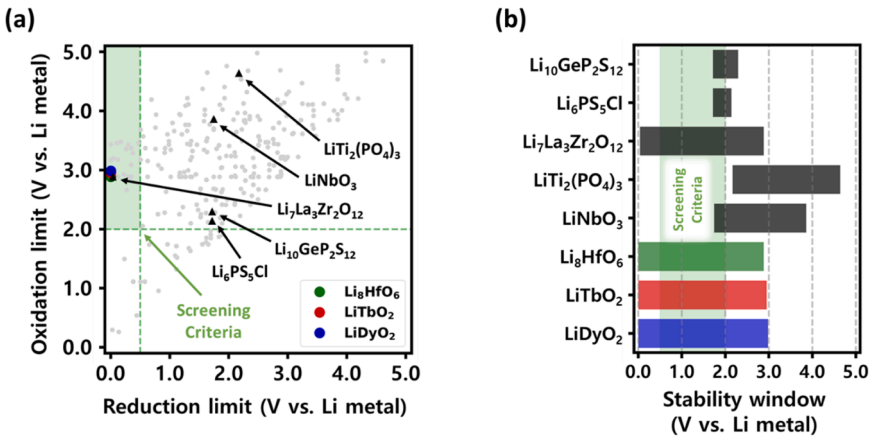

Fig. 3. Electrochemical stability window of coating candidates. (a) Reduction limit and oxidation limit of all Li-containing ternary oxides. Promising candidates are highlighted as a colored marker. (b) Electrochemical stability windows of some well-known SEs and promising anode coating candidates.

electrolyte, intimate and uniform contact must be maintained. However, during battery cycling, the dynamic difference between Li stripping at the interface and Li-atom diffusion from lithium metal bulk gradually leads to the formation of voids at the Li/SEs interfaces [44]. This reduction in interface contact area serves to polarize the battery cell, increases interfacial impedance, which can result in fostering dendrite growth and accelerating interface failure [45,46]. Poor Li wettability in many SEs, including LLZO, further complicates maintaining contact with Li metal, increasing the risk of dendrite growth [39,47,48]. Therefore, adding a strongly lithiophilic coating layer can address contact issues and suppress dendrite growth. To assess the lithiophilicity, we evaluated Li adsorption energies on coating surface [49]. Negative adsorption energy indicates strong interaction between Li and the coating, reflecting high lithiophilicity. Among various Li adsorption sites, the most stable configuration was used for adsorption energy analysis. Table S2 shows the results for 29 screened candidates, narrowed to 16 with lithiophilicity ($E_{ads} \leq 0$ eV) and stable interfaces with Li metal [49].

Various secondary interphases can form through interface reactions when lithium metal or SEs encounters the coating layer. These interfaces can be categorized by their electrical properties. Mixed electronically and ionically conducting interphases (MCI) transport both Li-ions and electrons, reducing high-valence cations in SEs and forming other MCI interphases, potentially depleting SEs or the anode [12,19,50], with LTPO being a representative example [51]. Thus, preventing MCI-type interphase formation is critical for ASSB operations [26,44,52]. Conversely, the solid-electrolyte interphase (SEI) can transport only Li^+ ions, preventing further lithiation and reduction of the SEs. Here, we focused on candidates that avoid MCI or metallic interphases, preventing electron injection into SEs and decomposition [39]

We examined reactions at both Li/coating and coating/SEs interfaces, considering SEs like $Li_{10}GeP_2S_{12}$, Li_6PS_5Cl, $Li_7La_3Zr_2O_{12}$, $LiTi_2(PO_4)_3$, and $LiNbO_3$. A representative Li-coating ($LiTbO_2$) – LGPS system is shown in Figure S2. Figures S2a-b compares MCI or metallic interphase formation with and without coating layer. Direct Li-SEs contact forms large unwanted interphases, including electronically conductive materials like Li-Ge compounds or Ge, which create conductive paths and transfer electrons to the electrolyte. Conversely, introducing a coating layer between the electrolyte and the electrode can reduce such MCI interphases, although some interphases may still form. Figures S2c-d detail interfacial reaction products and energies with and without $LiTbO_2$. Without a coating, interfacial reactions are energetically favorable, forming metallic interphases. Conversely, if an appropriate coating layer is applied, metallic interphases are not created, and the interface reaction driving force is relatively low. Therefore, an appropriate coating layer can act as a buffer layer between the electrolyte and the electrode. Candidates that pass this step include materials that do not generate metallic secondary phases at the Li metal-SE interface. Of the 16 structures screened, only three (Li_8HfO_6, $LiTbO_2$, and $LiDyO_2$) avoid electronically conductive phases with Li metal. Detailed interface reaction results are in Table S3.

2.5. Li-vacancy migration energy

Through the procedures so far, we selected Li_8HfO_6, $LiTbO_2$, and $LiDyO_2$ as candidates satisfying mechanical property, electrochemical stability and interface-related properties such as lithiophilicity and interface stability. However, if the coating layer has insufficient ionic conductivity, it can hinder overall battery performance [12]. Enhancing ionic conductivity can be achieved by increasing Li^+ carrier concentration through aliovalent doping or by introducing vacancies and cation disordering to open or expand Li^+ channels [53,54]. However, designing such materials is time-consuming and laborious, as super-ionic conduction is only activated in certain doping compositions with specific Li^+ sublattice ordering [55]. Thus, intrinsic ionic conductivity is arguably the most crucial among the various coating properties. The fundamental step in ionic diffusion is the migration of ions between stable sites through a higher energy environment [56]. The highest energy along this path is the activation energy for migration, which constitutes the main component of the activation energy for long-range diffusion in good ionic conductors. Previous studies suggest that a migration energy barrier lower than 0.7 eV would not impede overall Li^+ transport [57]. We identified all possible Li^+ ion transport paths in Li_8HfO_6, $LiTbO_2$, and $LiDyO_2$ and calculated their migration energy barriers using the climbing-image nudge elastic band (NEB) method [56,58].

The atomic structures, potential Li^+ transport pathways, and migration energy barriers for final candidates are illustrated in Fig. 4. Li_8HfO_6 (Fig. 4a) possesses a trigonal crystal structure with alternating layers of octahedral and tetrahedral layers. These layers consist of octahedral layers framed by HfO_6 polyhedra, with LiO_6 polyhedra filled between the frameworks, and tetrahedral layers filled only with LiO_4 polyhedra. Consequently, three possible pathways for Li^+ migration exist: octahedron to octahedron (Path 1), octahedron to tetrahedron (Path 2), and tetrahedron to tetrahedron (Path 3), shown in Fig. 4b. The migration energy for each pathway of Li_8HfO_6 is depicted in Fig. 4c. Among these pathways, migration to equivalent sites are Path 1 and Path 3. Path 1, from octahedron to octahedron, features the highest energy barrier among all paths, at 0.918 eV. In contrast, Path 3, from tetrahedron to tetrahedron, presents a lower energy barrier of 0.288 eV for Li^+ migration. Unlike the previous pathway, Path 2 (migration to a non-equivalent site) displays two migration energy barriers depending

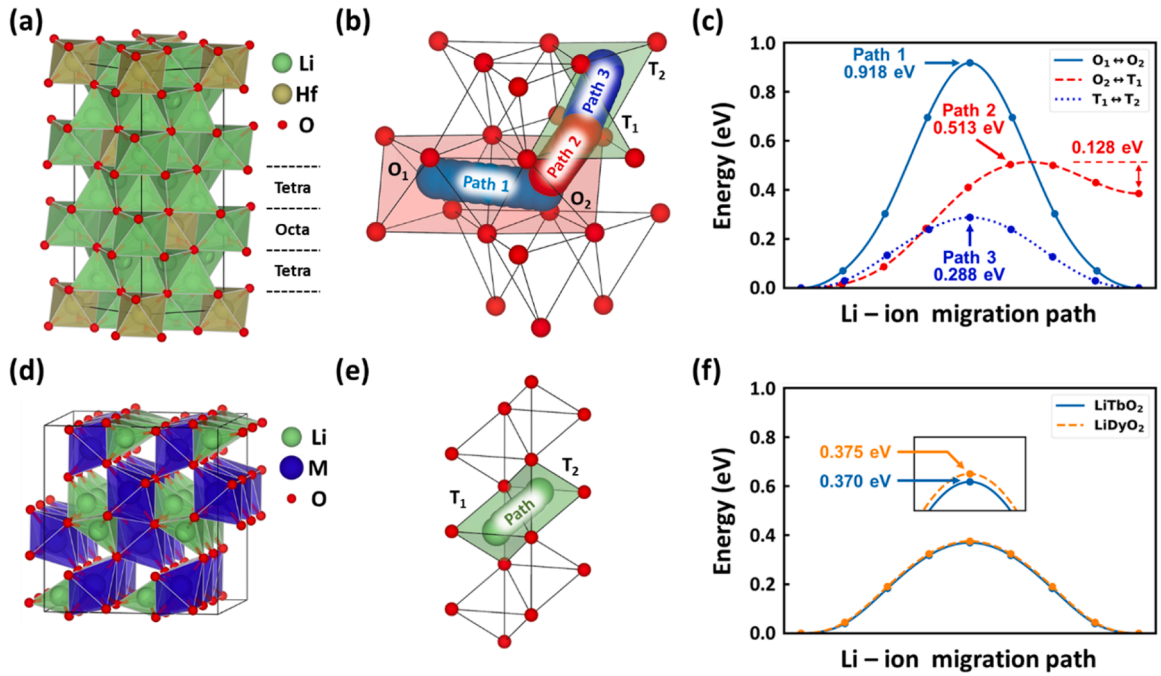

Fig. 4. (a) Atomic structure of the Li_8HfO_6. (b) Possible Li ion migration path of Li_8HfO_6. (c) Migration energy about Li_8HfO_6 of possible Li-ion path. (d) Atomic structure of the $LiMO_2$ (M = Tb and Dy). (e) Possible Li ion migration path of $LiMO_2$. (f) Migration energy about $LiMO_2$ of possible Li-ion path.

on the direction. The octahedron to tetrahedron pathway exhibits a moderate energy barrier of 0.513 eV, while the tetrahedron to octahedron pathway demonstrates the lowest migration energy barrier among the various pathways, at 0.128 eV. Thus, in the case of Li_8HfO_6, Li^+ transport within the crystal is expected to be hindered due to high energy barriers or asymmetric Li^+ migration energy barriers along the paths. $LiTbO_2$ and $LiDyO_2$ exhibit the same orthorhombic crystal structure (Fig. 4d), featuring a one-dimensional channel composed of LiO_4 tetrahedra within a framework of TbO_6, and DyO_6 octahedra. All Li atoms in the $LiTbO_2$, and $LiDyO_2$ channel exist at equivalent sites, resulting in a single transport pathway (Figure 4e). The Li^+ migration energy barrier for $LiMO_2$ is 0.370 eV and 0.375 eV for M corresponding to Tb and Dy, respectively (Fig. 4f). In comparison, other solid-state electrolytes such as LGPS, LPSCl, LTPO, and LATP show migration energy barriers of 0.17, 0.12, 0.94, and 0.19 eV, respectively. While the energy barriers of $LiTbO_2$ and $LiDyO_2$ are slightly higher compared to other electrolytes, excluding LTPO, considering factors such as compatibility with Li metal, lithiophilicity, and the small amount of material required, $LiMO_2$ is deemed suitable as a coating layer. This comparison is illustrated in Figure S3. As a result, the final anode coating candidates $LiTbO_2$ and $LiDyO_2$ were selected, and their various properties are shown in Table 1.

2.6. *Reaction-driven coating formation*

Synthesizing a coating layer separately requires additional processes, facilities, and costs. Alternatively, if the coating layer can be entirely induced from other materials, it could significantly reduce both cost and time. One of the unique characteristics of Li metal is its high reactivity [59], which can lead to the decomposition or chemical reaction of other materials. A notable example is the metal oxide surface coating (e.g., Al_2O_3 [60], ZrO_2 [61], and ZnO [62]) on NCM cathodes. These coatings are known to reduce side reactions and enhance Li^+ diffusion by improving interfacial stability between cathode materials and electrolytes. Among these, Al_2O_3 intrinsically has low Li^+ diffusivity, which theoretically increases interfacial resistance and reduces battery capacity and rate capability [63]. However, when applied, Al_2O_3 reacts with Li_2CO_3/LiOH byproducts on the material surface to partially form $LiAlO_2$, which has three-dimensional Li^+ diffusion channels [64]. This reaction not only stabilizes the cathode/electrolyte interface but also provides an efficient transport network for Li^+ extraction and intercalation, significantly enhancing electrochemical performance. Thus, our study aims to induce interface reaction to achieve the in-situ formation of coating layers.

To investigate the interface reaction between Li metal and binary precursors, we selected Tb_4O_7 and Dy_2O_3 as precursors. During battery operation, these precursors and Li metal may react in arbitrary amounts under room temperature and ambient atmospheric conditions. As shown in Fig. 5a-b, the interface reaction energies for the coating materials are -17 meV/atom for $LiTbO_2$ and -25 meV/atom for $LiDyO_2$. These negative reaction energies indicate that the target materials can be derived from the binary precursors. Additionally, phase diagrams for the Li-Tb-O and Li-Dy-O systems were constructed, as shown in Fig. 5c-d. To account for unknown ternary systems, we generated hypothetical ternary structures with a high probability of formation and incorporated them into the phase diagrams. From these diagrams, we observed that the target materials are more likely to form compared to other ternary structures, which appear as metastable phases.

Table 1
The various properties of the final candidates.

Material	mp-id	$E_{g,\ PBE}$ (eV)	E_{hull} (eV/atom)	G_{vrh} (GPa)	V_{red} (V)	V_{oxi} (V)	MCI formation	E_{ads} (eV)	E_m (eV)
$LiTbO_2$	mp-7137	4.55	0.000	55.86	0.00	2.96	X	- 1.66	0.370
$LiDyO_2$	mp-976726	4.56	0.000	60.05	0.00	2.98	X	- 1.97	0.375

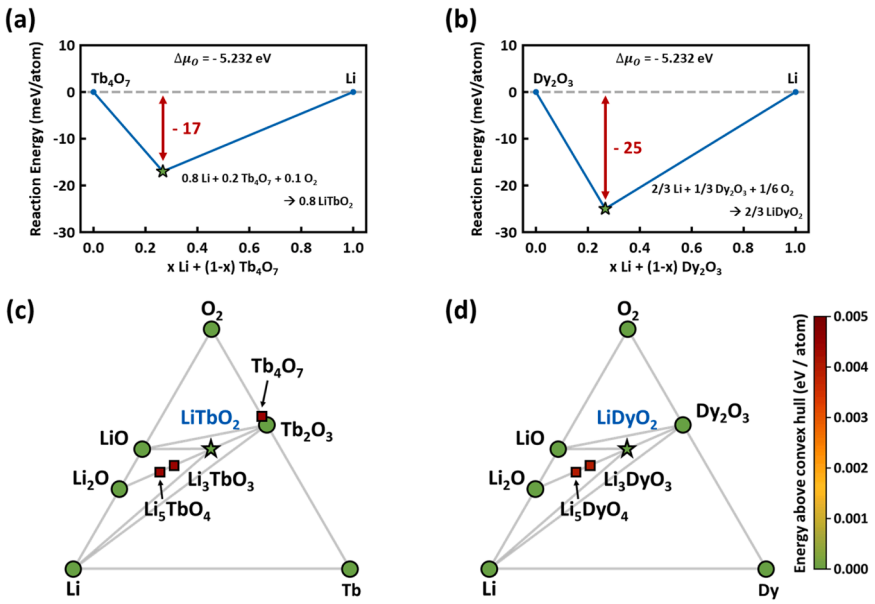

Fig. 5. Interface reaction energy plots for (a) the Li-Tb_4O_7 system and (b) the Li-Dy_2O_3 system. Phase diagrams of coating materials for (c) the Li-Tb-O system and (d) the Li-Dy-O system. The green, red-squared, and star-shaped markers represent thermodynamically stable, metastable, and promising coating candidates, respectively.

2.7. Experimental validation

To assess the electrochemical stability of ceramics selected as coating candidates, Tb_4O_7 and Dy_2O_3 were used as precursors for the coating layers. For comparison, boehmite (AlO(OH)), a conventional coating material, was used to highlight differences in electrochemical stability in Li-metal batteries. Figure 6f illustrates the configuration of the Li-Cu coin cells. To promote interfacial reactions with Li metal, each

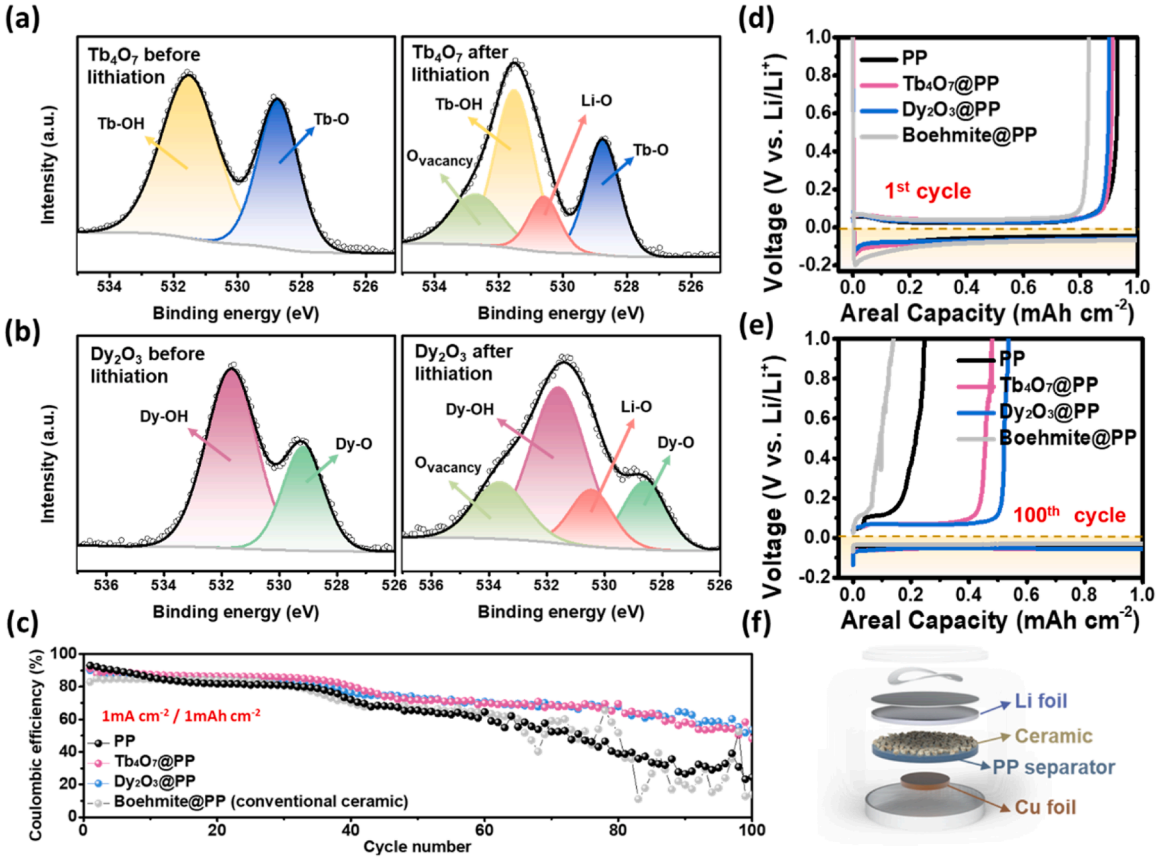

Fig. 6. XPS spectra comparison before and after lithiation of (a) Tb_4O_7 and (b) Dy_2O_3. (c) Cycling performance of cells with PP, Tb_4O_7@PP, Dy_2O_3@PP, and boehmite@PP at a current density of a 1 mA cm^{-2} and an areal capacity of 1 mAh cm^{-2}. Voltage profiles of each cell at the (d) 1st and (e) 100th cycles. (f) Schematic illustration of the cell configuration.

precursor was placed facing the Li anode, which was immersed in electrolyte under pressure and left overnight. The samples were then washed with fresh DEC solvent to remove any residues. After lithiation of the precursors, XPS analysis was performed before and after exposure to a Li-reactive environment. As shown in Fig. 6a-b, the Tb-OH and Dy-OH bond intensities decreased after lithiation, while new Li-O bonds were formed. These observations suggest that upon contact with Li metals, Tb_4O_7 and Dy_2O_3 undergo lithiation to form ternary compounds such as $LiTbO_2$ and $LiDyO_2$.

To examine whether the ionic conductivity enhancement of each material is reflected in experimental measurements beyond theoretical calculations, SUS|SUS symmetric cells were assembled and evaluated using EIS (Figure S4). The ohmic resistances of the cells employing pristine PP, Tb_4O_7@PP, and Dy_2O_3@PP were measured to be 4.35, 2.87, and 2.83 Ω, respectively. Based on these values, the corresponding ionic conductivities were calculated as 2.74×10^{-4}, 5.03×10^{-4}, and 5.10×10^{-4} S cm^{-1}, respectively. This result is consistent with the previously discussed computational predictions. They suggest that the use of Tb_4O_7 and Dy_2O_3 as anode coating materials can enhance ionic conductivity and contribute to improved electrochemical performance.

To investigate the potential effects of the coating layer on side reactions and electrochemical stability in Li-metal batteries, Li–Cu half-cells were fabricated and evaluated in an electrolyte of $LiPF_6$ in EC: DEC (1:1 by volume) at a current density of 1 mA cm^{-2} and an areal capacity of 1 mAh cm^{-2} (Fig. 6c). The Coulombic efficiency (CE) of the cell with the pristine polypropylene (PP) separator starts at 92% but decreases sharply after 40 cycles, reaching a low CE of 24.5% by the 100th cycle. In contrast, the cells with Tb_4O_7@PP and Dy_2O_3@PP maintain their initial CE values of 91.3% and 90.1%, respectively, and exhibit significantly improved CE values of 48.0% and 53.6% after 100 cycles. On the other hand, the cell with Boehmite@PP, a conventional ceramic-coated separator, consistently shows lower CEs than the cell with the pristine PP separator across all cycles, failing to demonstrate any substantial beneficial effect. The 1st and 100th galvanostatic discharge/charging voltage profiles of the respective cells are presented in Fig. 6d-e. In the 1st cycle, the discharge profiles of all the cells exhibit an initial sharp voltage drop below 0 V, indicating the occurrence of Li plating. Notably, no distinct plateau is observed in the voltage profiles of any cell, apart from the regions corresponding to Li plating and stripping, suggesting the absence of side reactions related to chemical or electrochemical degradation of the coating layer.

The effect of the coating layer on Li dendrite growth was examined by disassembling the Li–Cu cells before and after 10 cycles and observing the Li metal surface using top-view SEM (Fig. S5). The Li surface in the cell with bare PP exhibited randomly grown Li dendrites with non-uniform distribution, whereas the surfaces from the cells employing Tb_4O_7@PP and Dy_2O_3@PP showed relatively uniform and compact Li deposition. These observations suggest that the previously discussed advantages of Tb_4O_7 and Dy_2O_3 coatings help suppress lithium dendrite growth during cycling, thereby contributing to improved cell performance.

To evaluate the applicability of the ceramic coatings in practical cell configurations and under high-voltage conditions, Li–LFP cells employing each ceramic coated separator were assembled and tested within a voltage window of 2.5–4.0 V. Cycling performance was evaluated at a current density of 2 C for 100 cycles (Fig. S6a). The initial discharge capacities of the cells employing PP, Tb_4O_7@PP, and Dy_2O_3@PP were 137.2, 138.4, and 138.9 mAh g^{-1}, respectively, indicating slightly higher capacities for the cells using ceramic-coated separators. Stable cycling performance was observed in all cases, with capacity retention values exceeding 99.9% after 100 cycles. The distinct and stable voltage plateaus observed in the first charge–discharge profiles suggest that Tb_4O_7 and Dy_2O_3 coatings do not lead to side reactions under the high-voltage conditions of LFP cells (Figure S6b-d). Additionally, to investigate the effect of each ceramic coating on ionic conductivity enhancement, electrochemical performance was evaluated at various C-rates ranging from 0.1 to 4 C (Fig. S6e–h). At C-rates from 0.1 to 2 C, all cells exhibited similar discharge capacities. However, at 4 C, the cells employing Tb_4O_7@PP and Dy_2O_3@PP showed higher capacities compared to the cell with bare PP. These results clearly demonstrate that even in Li−LFP cell systems, the application of functional ceramic coatings can effectively enhance ionic conductivity, thereby contributing to superior performance under high-rate conditions.

Although Tb and Dy are categorized as rare earth elements and are generally more costly than conventional transition metals, their application in all-solid-state batteries is not fundamentally limited. This is because anode coatings are typically used in very small quantities compared to electrolytes, requiring only minimal material usage per cell. In addition, both Tb_4O_7 and Dy_2O_3 are studied as semiconductor materials [65,66], commercially available, and have established industrial supply chains, suggesting that their cost and scalability may be acceptable for practical implementation. Taking these factors together with our electrochemical results, we conclude that the Tb_4O_7- and Dy_2O_3-derived coating layers form stable interphase, enhancing the electrochemical stability of Li-containing cells through favorable interfacial properties, Li-ion mobility, and lithiophilicity. These findings support their potential as viable coating candidates for ASSBs.

3. Conclusions

In summary, this study successfully screened anode coating materials for Li all-solid-state batteries (ASSBs) using various methodologies, including high-throughput computational screening, Density Functional Theory (DFT), machine learning models, and Finite Element Method (FEM) simulations. This comprehensive approach identified several promising anode coating materials with desired properties, such as mechanical stability, non-reactivity with lithium metal, lithiophilicity, and moderate ionic conductivity. Moreover, by deriving the coating materials from binary precursors instead of synthesizing them separately, we demonstrated their practical applicability and performance. This result highlights the effectiveness of the combined screening process in addressing key challenges in solid-state battery technology, such as Li dendrite suppression and interface stability. These methodologies are expected to significantly advance ASSB development by offering a systematic framework for discovering and developing new functional materials, thereby enhancing the performance, safety, and commercial viability of next-generation energy storage solutions.

CRediT authorship contribution statement

Dong Won Jeon: Writing – original draft, Software, Methodology, Investigation, Formal analysis, Conceptualization. **Wootaek Choi:** Methodology, Investigation, Formal analysis. **Jun Hyuk Kang:** Methodology, Formal analysis. **Hyeon Woo Kim:** Software, Data curation. **Min Sung Kang:** Software, Formal analysis. **Woongchan Kim:** Software, Investigation. **Han Uk Lee:** Software, Formal analysis. **Hyunseok Ko:** Software, Funding acquisition. **Patrick Joohyun Kim:** Writing – review & editing, Project administration. **Sung Beom Cho:** Writing – review & editing, Supervision, Project administration, Funding acquisition.

Declaration of competing interest

The authors declare that they have no known competing financial interests or personal relationships that could have appeared to influence the work reported in this paper.

Acknowledgements

Computational resources were supported by the Korea Supercomputing Center (No. KSC-2023-CRE-0387, KSC-2024-CRE-0467 and No. KSC-2024-CRE-0049). This work is supported by the National R&D

Program through the National Research Foundation of Korea (NRF) funded by the Ministry of Science and ICT (No. RS-2024-00407282, and No. RS-2024-00444182).

Supplementary materials

Supplementary material associated with this article can be found, in the online version, at doi:10.1016/j.apsadv.2025.100842.

Data availability

Data will be made available on request.

References

[1] W. Li, J.R. Dahn, D.S. Wainwright, Rechargeable lithium batteries with aqueous electrolytes, Science 264 (1994) 1115–1118, https://doi.org/10.1126/science.264.5162.1115.

[2] N. Kamaya, K. Homma, Y. Yamakawa, M. Hirayama, R. Kanno, M. Yonemura, T. Kamiyama, Y. Kato, S. Hama, K. Kawamoto, A. Mitsui, A lithium superionic conductor, Nat. Mater. 10 (2011) 682–686, https://doi.org/10.1038/nmat3066.

[3] Y. Kato, S. Hori, T. Saito, K. Suzuki, M. Hirayama, A. Mitsui, M. Yonemura, H. Iba, R. Kanno, High-power all-solid-state batteries using sulfide superionic conductors, Nat. Energy 1 (2016) 16030, https://doi.org/10.1038/nenergy.2016.30.

[4] M. Tatsumisago, M. Nagao, A. Hayashi, Recent development of sulfide solid electrolytes and interfacial modification for all-solid-state rechargeable lithium batteries, J. Asian Ceram. Soc. 1 (2013) 17–25, https://doi.org/10.1016/j.jascer.2013.03.005.

[5] K. (Kelvin) Fu, Y. Gong, B. Liu, Y. Zhu, S. Xu, Y. Yao, W. Luo, C. Wang, S.D. Lacey, J. Dai, Y. Chen, Y. Mo, E. Wachsman, L. Hu, Toward garnet electrolyte–based Li metal batteries: an ultrathin, highly effective, artificial solid-state electrolyte/metallic Li interface, Sci. Adv. 3 (2017) e1601659, https://doi.org/10.1126/sciadv.1601659.

[6] C. Cao, Z.-B. Li, X.-L. Wang, X.-B. Zhao, W.-Q. Han, Recent advances in inorganic solid electrolytes for lithium batteries, Front. Energy Res. 2 (2014) 25, https://doi.org/10.3389/fenrg.2014.00025.

[7] J.C. Bachman, S. Muy, A. Grimaud, H.-H. Chang, N. Pour, S.F. Lux, O. Paschos, F. Maglia, S. Lupart, P. Lamp, L. Giordano, Y. Shao-Horn, Inorganic solid-State electrolytes for lithium batteries: mechanisms and properties governing ion conduction, Chem. Rev. 116 (2016) 140–162, https://doi.org/10.1021/acs.chemrev.5b00563.

[8] A. Manthiram, X. Yu, S. Wang, Lithium battery chemistries enabled by solid-state electrolytes, Nat. Rev. Mater. 2 (2017) 16103, https://doi.org/10.1038/natrevmats.2016.103.

[9] K. Kerman, A. Luntz, V. Viswanathan, Y.-M. Chiang, Z. Chen, Review—Practical challenges hindering the development of solid State Li ion batteries, J. Electrochem. Soc. 164 (2017) A1731–A1744, https://doi.org/10.1149/2.1571707jes.

[10] J. Kasemchainan, S. Zekoll, D.S. Jolly, Z. Ning, G.O. Hartley, J. Marrow, P. G. Bruce, Critical stripping current leads to dendrite formation on plating in lithium anode solid electrolyte cells, Nat. Mater. 18 (2019) 1105–1111, https://doi.org/10.1038/s41563-019-0438-9.

[11] T. Famprikis, P. Canepa, J.A. Dawson, M.S. Islam, C. Masquelier, Fundamentals of inorganic solid-state electrolytes for batteries, Nat. Mater. 18 (2019) 1278–1291, https://doi.org/10.1038/s41563-019-0431-3.

[12] X. Miao, S. Guan, C. Ma, L. Li, C. Nan, Role of interfaces in solid-State batteries, Adv. Mater. 35 (2023) e2206402, https://doi.org/10.1002/adma.202206402.

[13] X. Li, J. Liu, M.N. Banis, A. Lushington, R. Li, M. Cai, X. Sun, Atomic layer deposition of solid-state electrolyte coated cathode materials with superior high-voltage cycling behavior for lithium ion battery application, Energy Environ. Sci. 7 (2013) 768–778, https://doi.org/10.1039/c3ee42704h.

[14] Z.-J. Zhang, S.-L. Chou, Q.-F. Gu, H.-K. Liu, H.-J. Li, K. Ozawa, J.-Z. Wang, Enhancing the high rate capability and cycling stability of LiMn2O4 by coating of solid-State electrolyte LiNbO3, ACS Appl. Mater. Interfaces 6 (2014) 22155–22165, https://doi.org/10.1021/am5056504.

[15] X. Han, Y. Gong, K. (Kelvin) Fu, X. He, G.T. Hitz, J. Dai, A. Pearse, B. Liu, H. Wang, G. Rubloff, Y. Mo, V. Thangadurai, E.D. Wachsman, L. Hu, Negating interfacial impedance in garnet-based solid-state Li metal batteries, Nat. Mater. 16 (2017) 572–579, https://doi.org/10.1038/nmat4821.

[16] C. Wang, K. Fu, S.P. Kammampata, D.W. McOwen, A.J. Samson, L. Zhang, G. T. Hitz, A.M. Nolan, E.D. Wachsman, Y. Mo, V. Thangadurai, L. Hu, Garnet-type solid-State electrolytes: materials, interfaces, and batteries, Chem. Rev. 120 (2020) 4257–4300, https://doi.org/10.1021/acs.chemrev.9b00427.

[17] X. Hao, Q. Zhao, S. Su, S. Zhang, J. Ma, L. Shen, Q. Yu, L. Zhao, Y. Liu, F. Kang, Y. He, Constructing multifunctional interphase between Li1.4Al0.4Ti1.6(PO4)3 and Li metal by magnetron sputtering for highly stable solid-State lithium metal batteries, Adv. Energy Mater. 9 (2019), https://doi.org/10.1002/aenm.201901604.

[18] C.-L. Tsai, V. Roddatis, C.V. Chandran, Q. Ma, S. Uhlenbruck, M. Bram, P. Heitjans, O. Guillon, Li7La3Zr2O12 Interface modification for Li dendrite prevention, ACS Appl. Mater. Interfaces 8 (2016) 10617–10626, https://doi.org/10.1021/acsami.6b00831.

[19] R. Chen, Q. Li, X. Yu, L. Chen, H. Li, Approaching practically accessible solid-State batteries: stability issues related to solid electrolytes and interfaces, Chem. Rev. 120 (2020) 6820–6877, https://doi.org/10.1021/acs.chemrev.9b00268.

[20] A. Jain, S.P. Ong, G. Hautier, W. Chen, W.D. Richards, S. Dacek, S. Cholia, D. Gunter, D. Skinner, G. Ceder, K.A. Persson, 04. Commentary: The Materials Project: A materials genome approach to accelerating materials innovation, APL Mater 1 (2013) 011002, https://doi.org/10.1063/1.4812323.

[21] M.A. Green, Intrinsic concentration, effective densities of states, and effective mass in silicon, J. Appl. Phys. 67 (1990) 2944–2954, https://doi.org/10.1063/1.345414.

[22] Y. Xiao, L.J. Miara, Y. Wang, G. Ceder, Computational screening of cathode coatings for solid-State batteries, Joule 3 (2019) 1252–1275, https://doi.org/10.1016/j.joule.2019.02.006.

[23] S. Yu, H. Park, D.J. Siegel, Thermodynamic assessment of coating materials for solid-State Li, Na, and K batteries, ACS Appl. Mater. Interfaces 11 (2019) 36607–36615, https://doi.org/10.1021/acsami.9b11001.

[24] H. Liu, X.-B. Cheng, J.-Q. Huang, H. Yuan, Y. Lu, C. Yan, G.-L. Zhu, R. Xu, C.-Z. Zhao, L.-P. Hou, C. He, S. Kaskel, Q. Zhang, Controlling dendrite growth in solid-State electrolytes, ACS Energy Lett. 5 (2020) 833–843, https://doi.org/10.1021/acsenergylett.9b02660.

[25] D. Cao, X. Sun, Q. Li, A. Natan, P. Xiang, H. Zhu, Lithium dendrite in all-solid-State batteries: growth mechanisms, suppression strategies, and characterizations, Matter 3 (2020) 57–94, https://doi.org/10.1016/j.matt.2020.03.015.

[26] K.J. Kim, M. Balaish, M. Wadaguchi, L. Kong, J.L.M. Rupp, Solid-State Li–Metal batteries: challenges and horizons of oxide and sulfide Solid electrolytes and their interfaces, Adv. Energy Mater. 11 (2021), https://doi.org/10.1002/aenm.202002689.

[27] C. Monroe, J. Newman, The impact of elastic deformation on deposition kinetics at lithium/polymer interfaces, J. Electrochem. Soc. 152 (2005) A396–A404, https://doi.org/10.1149/1.1850854.

[28] C. Wang, G. Bai, Y. Yang, X. Liu, H. Shao, Dendrite-free all-solid-state lithium batteries with lithium phosphorous oxynitride-modified lithium metal anode and composite solid electrolytes, Nano Res. 12 (2019) 217–223, https://doi.org/10.1007/s12274-018-2205-7.

[29] Z. Deng, Z. Wang, I.-H. Chu, J. Luo, S.P. Ong, Elastic properties of Alkali superionic conductor electrolytes from first principles calculations, J. Electrochem. Soc. 163 (2016) A67–A74, https://doi.org/10.1149/2.0061602jes.

[30] J.E. Ni, E.D. Case, J.S. Sakamoto, E. Rangasamy, J.B. Wolfenstine, Room temperature elastic moduli and Vickers hardness of hot-pressed LLZO cubic garnet, J. Mater. Sci. 47 (2012) 7978–7985, https://doi.org/10.1007/s10853-012-6687-5.

[31] C. Monroe, J. Newman, The effect of interfacial deformation on electrodeposition kinetics, J. Electrochem. Soc. 151 (2004) A880–A886, https://doi.org/10.1149/1.1710893.

[32] Z. Ahmad, V. Viswanathan, Stability of electrodeposition at solid-solid interfaces and implications for metal anodes, Phys. Rev. Lett. 119 (2017) 056003, https://doi.org/10.1103/physrevlett.119.056003.

[33] M. de Jong, W. Chen, T. Angsten, A. Jain, R. Notestine, A. Gamst, M. Sluiter, C. K. Ande, S. van der Zwaag, J.J. Plata, C. Toher, S. Curtarolo, G. Ceder, K. A. Persson, M. Asta, Charting the complete elastic properties of inorganic crystalline compounds, Sci. Data 2 (2015) 150009, https://doi.org/10.1038/sdata.2015.9.

[34] S. Curtarolo, G.L.W. Hart, M.B. Nardelli, N. Mingo, S. Sanvito, O. Levy, The high-throughput highway to computational materials design, Nat. Mater. 12 (2013) 191–201, https://doi.org/10.1038/nmat3568.

[35] M. Wen, M.K. Horton, J.M. Munro, P. Huck, K.A. Persson, An equivariant graph neural network for the elasticity tensors of all seven crystal systems, Digit. Discov. (2024), https://doi.org/10.1039/d3dd00233k.

[36] X. Liu, R. Garcia-Mendez, A.R. Lupini, Y. Cheng, Z.D. Hood, F. Han, A. Sharafi, J. C. Idrobo, N.J. Dudney, C. Wang, C. Ma, J. Sakamoto, M. Chi, Local electronic structure variation resulting in Li 'filament' formation within solid electrolytes, Nat. Mater. 20 (2021) 1485–1490, https://doi.org/10.1038/s41563-021-01019-x.

[37] M.W. Schulze, L.D. McIntosh, M.A. Hillmyer, T.P. Lodge, High-modulus, high-conductivity nanostructured polymer electrolyte membranes via polymerization-induced phase separation, Nano Lett. 14 (2014) 122–126, https://doi.org/10.1021/nl4034818.

[38] P. Barai, K. Higa, V. Srinivasan, Lithium dendrite growth mechanisms in polymer electrolytes and prevention strategies, Phys. Chem. Chem. Phys. 19 (2017) 20493–20505, https://doi.org/10.1039/c7cp03304d.

[39] Y. Xiao, Y. Wang, S.-H. Bo, J.C. Kim, L.J. Miara, G. Ceder, Understanding interface stability in solid-state batteries, Nat. Rev. Mater. 5 (2020) 105–126, https://doi.org/10.1038/s41578-019-0157-5.

[40] W.D. Richards, L.J. Miara, Y. Wang, J.C. Kim, G. Ceder, Interface stability in solid-State batteries, Chem. Mater. 28 (2016) 266–273, https://doi.org/10.1021/acs.chemmater.5b04082.

[41] S.P. Ong, L. Wang, B. Kang, G. Ceder, Li−Fe−P−O2 phase diagram from first principles calculations, Chem. Mater. 20 (2008) 1798–1807, https://doi.org/10.1021/cm702327g.

[42] S.P. Ong, A. Jain, G. Hautier, B. Kang, G. Ceder, Thermal stabilities of delithiated olivine MPO4 (M=Fe, Mn) cathodes investigated using first principles calculations, Electrochem. Commun. 12 (2010) 427–430, https://doi.org/10.1016/j.elecom.2010.01.010.

[43] Z. Yu, C. Gan, A.S. Mijailovic, A. Stone, R. Hurt, C.L. Pernia, X. Xiao, C. Shi, B. W. Sheldon, Lithium dendrite deflection at mixed ionic–Electronic conducting interlayers in solid electrolytes, Adv. Energy Mater. 15 (2025), https://doi.org/10.1002/aenm.202403179.

[44] J. Liu, H. Yuan, H. Liu, C. Zhao, Y. Lu, X. Cheng, J. Huang, Q. Zhang, Unlocking the failure mechanism of solid State lithium metal batteries, Adv. Energy Mater. 12 (2022), https://doi.org/10.1002/aenm.202100748.
[45] T. Krauskopf, H. Hartmann, W.G. Zeier, J. Janek, Toward a fundamental understanding of the lithium metal anode in solid-State batteries an electrochemo-mechanical study on the garnet-type solid electrolyte Li6.25Al0.25La3Zr2O12, ACS Appl. Mater. Interfaces 11 (2019) 14463–14477, https://doi.org/10.1021/acsami.9b02537.
[46] T. Krauskopf, B. Mogwitz, H. Hartmann, D.K. Singh, W.G. Zeier, J. Janek, The fast charge transfer kinetics of the lithium metal anode on the garnet-type solid electrolyte Li6.25Al0.25La3Zr2O12, Adv. Energy Mater. 10 (2020), https://doi.org/10.1002/aenm.202000945.
[47] A. Banerjee, X. Wang, C. Fang, E.A. Wu, Y.S. Meng, Interfaces and interphases in all-solid-State batteries with inorganic solid electrolytes, Chem. Rev. 120 (2020) 6878–6933, https://doi.org/10.1021/acs.chemrev.0c00101.
[48] D. Wang, C. Zhu, Y. Fu, X. Sun, Y. Yang, Interfaces in garnet-based all-solid-State lithium batteries, Adv. Energy Mater. 10 (2020), https://doi.org/10.1002/aenm.202001318.
[49] Z. Chen, W. Chen, H. Wang, C. Zhang, X. Qi, L. Qie, F. Wu, L. Wang, F. Yu, Lithiophilic anchor points enabling endogenous symbiotic Li3N interface for homogeneous and stable lithium electrodeposition, Nano Energy 93 (2022) 106836, https://doi.org/10.1016/j.nanoen.2021.106836.
[50] B. Dunn, H. Kamath, J.-M. Tarascon, Electrical energy storage for the grid: A battery of choices, Science 334 (2011) 928–935, https://doi.org/10.1126/science.1212741.
[51] B. Lang, B. Ziebarth, C. Elsässer, Lithium ion conduction in LiTi2(PO4)3 and related compounds based on the NASICON structure: A first-principles study, Chem. Mater. 27 (2015) 5040–5048, https://doi.org/10.1021/acs.chemmater.5b01582.
[52] M. Gauthier, T.J. Carney, A. Grimaud, L. Giordano, N. Pour, H.-H. Chang, D. P. Fenning, S.F. Lux, O. Paschos, C. Bauer, F. Maglia, S. Lupart, P. Lamp, Y. Shao-Horn, Electrode–Electrolyte interface in Li-ion batteries: current understanding and new insights, J. Phys. Chem. Lett. 6 (2015) 4653–4672, https://doi.org/10.1021/acs.jpclett.5b01727.
[53] Y.-C. Yin, J.-T. Yang, J.-D. Luo, G.-X. Lu, Z. Huang, J.-P. Wang, P. Li, F. Li, Y.-C. Wu, T. Tian, Y.-F. Meng, H.-S. Mo, Y.-H. Song, J.-N. Yang, L.-Z. Feng, T. Ma, W. Wen, K. Gong, L.-J. Wang, H.-X. Ju, Y. Xiao, Z. Li, X. Tao, H.-B. Yao, A LaCl3-based lithium superionic conductor compatible with lithium metal, Nature 616 (2023) 77–83, https://doi.org/10.1038/s41586-023-05899-8.
[54] S. Yu, J. Noh, B. Kim, J.-H. Song, K. Oh, J. Yoo, S. Lee, S.-O. Park, W. Kim, B. Kang, D. Kil, K. Kang, Design of a trigonal halide superionic conductor by regulating cation order-disorder, Science 382 (2023) 573–579, https://doi.org/10.1126/science.adg6591.
[55] X. He, Y. Zhu, Y. Mo, Origin of fast ion diffusion in super-ionic conductors, Nat. Commun. 8 (2017) 15893, https://doi.org/10.1038/ncomms15893.
[56] Y. Wang, W.D. Richards, S.P. Ong, L.J. Miara, J.C. Kim, Y. Mo, G. Ceder, Design principles for solid-state lithium superionic conductors, Nat. Mater. 14 (2015) 1026–1031, https://doi.org/10.1038/nmat4369.
[57] T. Lu, S. Meng, M. Liu, Electrochemically and chemically stable electrolyte–electrode interfaces for lithium iron phosphate all-solid-state batteries with sulfide electrolytes, J. Mater. Chem. A (2024), https://doi.org/10.1039/d3ta06227a.
[58] G. Henkelman, B.P. Uberuaga, H. Jónsson, A climbing image nudged elastic band method for finding saddle points and minimum energy paths, J. Chem. Phys. 113 (2000) 9901–9904, https://doi.org/10.1063/1.1329672.
[59] C. Ma, Y. Cheng, K. Yin, J. Luo, A. Sharafi, J. Sakamoto, J. Li, K.L. More, N. J. Dudney, M. Chi, Interfacial stability of Li metal–Solid electrolyte elucidated via in situ electron microscopy, Nano Lett. 16 (2016) 7030–7036, https://doi.org/10.1021/acs.nanolett.6b03223.
[60] N. Su, Y. Lyu, R. Gu, B. Guo, Al2O3 coated Li1.2Ni0.2Mn0.2Ru0.4O2 as cathode material for Li-ion batteries, J. Alloy. Compd. 741 (2018) 398–403, https://doi.org/10.1016/j.jallcom.2018.01.146.
[61] T. Tao, C. Chen, Y. Yao, B. Liang, S. Lu, Y. Chen, Enhanced electrochemical performance of ZrO2 modified LiNi0.6Co0.2Mn0.2O2 cathode material for lithium ion batteries, Ceram. Int. 43 (2017) 15173–15178, https://doi.org/10.1016/j.ceramint.2017.08.048.
[62] J.-Z. Kong, C. Ren, G.-A. Tai, X. Zhang, A.-D. Li, D. Wu, H. Li, F. Zhou, Ultrathin ZnO coating for improved electrochemical performance of LiNi0.5Co0.2Mn0.3O2 cathode material, J. Power Sources 266 (2014) 433–439, https://doi.org/10.1016/j.jpowsour.2014.05.027.
[63] W. Tang, Z. Chen, F. Xiong, F. Chen, C. Huang, Q. Gao, T. Wang, Z. Yang, W. Zhang, An effective etching-induced coating strategy to shield LiNi0.8Co0.1Mn0.1O2 electrode materials by LiAlO2, J. Power Sources 412 (2019) 246–254, https://doi.org/10.1016/j.jpowsour.2018.11.062.
[64] S. Dong, Y. Zhou, C. Hai, J. Zeng, Y. Sun, Y. Ma, Y. Shen, X. Li, X. Ren, C. Sun, G. Zhang, Z. Wu, Enhanced cathode performance: mixed Al2O3 and LiAlO2 coating of Li1.2Ni0.13Co0.13Mn0.54O2, ACS Appl. Mater. Interfaces 12 (2020) 38153–38162, https://doi.org/10.1021/acsami.0c10459.
[65] A. Cherif, S. Alotaibi, H. Saghrouni, L. Beji, Improvement of physical properties of MOS devices based on rare earth oxides, AIP Adv. 13 (2023) 025042, https://doi.org/10.1063/5.0135129.
[66] A.A. Sifawa, S.M. Mohammad, A. Muhammad, S.M. Abed, W.F. Lim, Influence of different annealing ambient on terbium oxide passivation layers sputtered using the RF sputtering on silicon substrate, Nano Express 5 (2024) 025023, https://doi.org/10.1088/2632-959x/ad52b4.